Wavelet analysis of variability in annual Canadian streamflows

Paulin Coulibaly

Department of Civil Engineering and School of Geography and Geology, McMaster University, Hamilton, Ontario, Canada

Donald H. Burn

Department of Civil Engineering, University of Waterloo, Waterloo, Ontario, Canada

Received 9 September 2003; revised 15 December 2003; accepted 26 January 2004; published 16 March 2004.

[1] Wavelet analysis is used to identify and describe variability in annual Canadian streamflows and to gain insights into the dynamical link between the streamflows and the dominant modes of climate variability in the Northern Hemisphere. Results from applying continuous wavelet transform to mean annual streamflows from 79 rivers selected from the Canadian Reference Hydrometric Basin Network (RHBN) reveal striking climate-related features before the 1950s and after the 1970s. The span of available observations, 1911–1999, allows for depicting variance for periods up to 12 years. Scale-averaged wavelet power spectra are used to simultaneously assess the interannual and spatial variability in 79 annual streamflow time series. The most striking feature, in the 2–3 year band and in the 3–6 year band (the 6–12 year band is dominated by white noise (since 1950) and is not considered further) is a net distinction between the timing and intensity of the interannual variability in western, central, and eastern streamflows, which is shown to be linked to the regional climatology. It is found that for the 2–3 year band, the Canadian streamflows are depicted mainly by the Pacific North America (PNA) during 1950–1999, and the Northern Hemisphere Annular Mode (NAM) only prior to 1950, and the North Atlantic Oscillation (NAO) after 1970. Similarly, in the 3–6 year band, the streamflows are depicted mostly by the NAO, the sea surface temperature anomalies over the Niño-3 region (ENSO3) and the PNA during the period 1950–1999, and the NAM prior to 1950. Furthermore, strong local correlations between teleconnection patterns and western, central, and eastern streamflows are also revealed in both the 2–3 and 3–6 year bands with striking changes around 1950 and 1970. The correlation analysis in the 2–3 year and 3–6 year bands revealed the presence of two change points in the west and east streamflows occurring around 1950 and 1970. *INDEX TERMS:* 1860 Hydrology: Runoff and streamflow; 1833 Hydrology: Hydroclimatology; 3220 Mathematical Geophysics: Nonlinear dynamics; *KEYWORDS:* streamflows, wavelet analysis, space-time variability, climatic patterns, change point

Citation: Coulibaly, P., and D. H. Burn (2004), Wavelet analysis of variability in annual Canadian streamflows, *Water Resour. Res.*, *40*, W03105, doi:10.1029/2003WR002667.

1. Introduction

[2] Recent advances in the identification of coherent climatic patterns in the atmospheric circulation can be particularly relevant to the interpretation of variations and long-range persistence within hydrological records. Low-frequency climatic fluctuations reflect locally on the interannual variability in hydroclimatic variables (temperature, precipitation, river flow) which are key elements in understanding the underlying dynamics of the hydrologic cycle. Furthermore, a better understanding of the temporal and local/regional connection between low-frequency climatic fluctuations and the variations of river discharge can lead to better hydrologic system modeling (e.g., improved long-range forecast) and hence improved water resources management. However, assessing the changes in atmospheric patterns and their relationships to the Northern Hemisphere hydrologic regime remains a difficult task owing to the coarseness of the ground station network even for a standard variable such as precipitation. The space-time variability of precipitation (solid and liquid) requires a large number of weather stations for a proper characterization of rainfall or snowfall patterns over large areas such as Canadian watersheds. As an alternative, one can resort to river discharge records. Hydrological systems act as spatial and temporal integrators of precipitation over specific watersheds, and hence annual river flow observations can serve as a pertinent index of interannual hydroclimatic variability at a local or regional scale.

[3] This study aims to assess the variability of Canadian annual streamflows and the possible links to the dominant climatic patterns in the Northern Hemisphere. Most previous interannual variability assessment studies are based either on direct correlation analysis to identify strong statistical relationship between the hydroclimatic variable and the teleconnection pattern indices [e.g., *Yarnal and Diaz*, 1986; *Redmond and Koch*, 1991] or more recently

Copyright 2004 by the American Geophysical Union.
0043-1397/04/2003WR002667$09.00

on nonparametric multitaper method of spectral analysis [*Rajagopalan and Lall*, 1998], a more direct measure of the occurrence process. All these approaches assume stationary time series, but continuous wavelet analysis has revealed that the interannual variability of phenomena such as El Niño-Southern Oscillation (ENSO) and the North Atlantic Oscillation (NAO) are nonstationary processes, since their variance changes in frequency and intensity through time [e.g., *Torrence and Compo*, 1998; *Higuchi et al.*, 1999; *Coulibaly et al.*, 2000]. Wavelet analysis has been used in geophysics and meteorology to identify coherent convective storm structures and characterize their temporal variability [*Kumar and Foufoula-Georgiou*, 1993; *Takeuchi et al.*, 1994; *Kumar*, 1996; *Szilagyi et al.*, 1999] or to analyze localized variations within geophysical time series including climatic indices [*Shabbar et al.*, 1997b; *Hu et al.*, 1998; *Lucero and Rodriguez*, 1999]. In the field of hydrology, wavelet analysis has been recently applied to examine daily rainfall-runoff relationships in a karstic watershed [*Labat et al.*, 2000] and also to characterize daily streamflow [*Smith et al.*, 1998; *Saco and Kumar*, 2000] and monthly reservoir inflow [*Coulibaly et al.*, 2000].

[4] The main objectives of this analysis are to describe and document the variability in annual Canadian streamflows using wavelet analysis. This study also aims to examine the role of the dominant climatic patterns in the Northern Hemisphere on the interannual variability of Canadian streamflows. The remainder of the paper is organized as follows. A description of the study area and the data sets are first provided. The continuous wavelet analysis method is presented next. Results from the wavelet analysis are then reported, and finally some conclusions are drawn.

2. Study Area and Data Sets

2.1. Reference Hydrometric Basin Network (RHBN)

[5] The analysis described herein was performed on stations from the Reference Hydrometric Basin Network (RHBN), a data collection network of natural rivers in Canada identified by Environment Canada for climatic change research. The five criteria according to which stations were selected for the RHBN are as follows [*Harvey et al.*, 1999]:

[6] First is the degree of basin development. Stations that were included in the network were those that reflect catchments that are pristine or have stable land-use conditions. As a guideline, a catchment that has less than 10% of its surface area modified from natural conditions was considered to represent pristine conditions.

[7] Second is the absence of significant regulations or diversions. A catchment was considered natural if there was no control structure upstream of the gauging station, and it was considered regulated if there was an upstream control structure.

[8] Third is record length. A station must have a minimum record length of 20 years to be included in the RHBN. This record length was chosen to make sure that underrepresented climatic or geographic areas, which are characterized by minimal data availability, were included in the network. The present work selected from the RHBN only those stations with a record length of at least 35 years to ensure an adequate record length for the wavelet analysis.

[9] Fourth is longevity. This criterion was based on the judgment of the regional staff. A station was excluded from the network if it is currently active but was expected not to have future data collection activities.

[10] Fifth is data accuracy. Data accuracy was assessed qualitatively by local experts based on knowledge of the hydraulic condition of the stations to ensure that only stations with good quality data were included in the network.

[11] The RHBN originally consisted of 255 hydrometric stations. All stations had at least 20 years of record, with an average record length of 38 years. Basin sizes range from 3.63 to 145,000 km^2, with a median size of 1170 km^2; 10% of the basins have a drainage area greater than 20,000 km^2; and 10% have a drainage area less than 100 km^2. The RHBN has decreased in size from its original design and currently contains 200 + stations. An analysis of the characteristics of stations within the RHBN indicates certain limitations of the existing network. The network tends to comprise large basins in the north and smaller basins in the south, and certain provinces have large gaps in spatial coverage.

[12] The current research employs a subset of the RHBN consisting of 79 longer-term gauging stations (see Figure 1) to minimize the limited data record problem and allow longer period (up to decadal timescale) analysis. It can be seen that the subset of the RHBN that has been selected for this work suffers from the same limitations outlined above for the RHBN as a whole. In particular, there is a limited number of stations representing the Canadian north and there are few stations from the Prairie Provinces. The median record length for the stations analyzed in this work is 49 years, with a range of record lengths from 35 to 85 years. The catchment drainage areas range from 3.63 to 29,900 km^2, with a median value of 1350 km^2. As such, the subset of the RHBN is fairly typical of the stations in the RHBN in terms of drainage areas, but consists only of the best available streamflow time series with longer record length. The selected sites along with the station numbers, drainage basin areas, and locations are listed in Table 1. The regional grouping of sites (Table 1) is based on statistical analysis and climatic factors [*Harvey et al.*, 1999; *Adamowski and Bocci*, 2001]. The hydrologic variable selected for this research is the annual mean flow given that the study is mainly concerned with interannual to decadal variability in the streamflows. Note that using annual mean flow eliminates the strong seasonal variability inherent to Nordic river flows.

2.2. Selected Climatic Indices

[13] The analysis also includes several climatic patterns that appear and persist in the Northern Hemisphere. Two of these are the North Atlantic Oscillation (NAO) and the Pacific-North American (PNA) that are found to be the predominant patterns for displaying low-frequency variability (interannual to decadal timescales) in the Northern Hemisphere (e.g., storm-track and temperature changes [*Barnston and Livezey*, 1987; *Lamb and Peppler*, 1987; *National Research Council*, 1998]). The NAO is a large-scale alternation of atmospheric mass with centers of action near the Icelandic Low and the Azores High. It is the dominant and persistent mode of atmospheric behavior in the North Atlantic throughout the year, explaining on average 32% of the variance in monthly sea level pressures (SLP) [*Cayan*, 1992] but with even greater dominance during the winter. The NAO index used in this study is

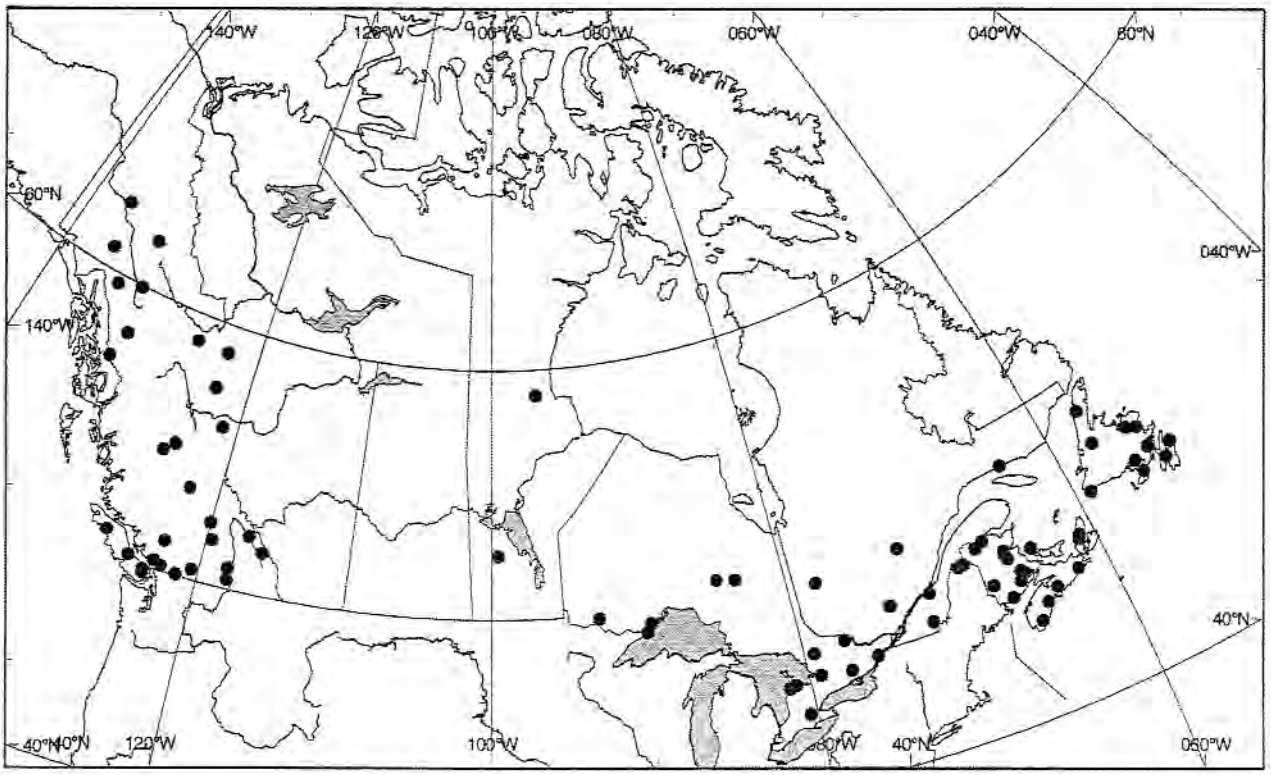

Figure 1. Location map of the 79 Canadian Reference Hydrometric Basin Network (RHBN) flow stations selected.

from *Hurrell* [1995], who exploited SLP anomalies from Lisbon, Portugal, and Stykkisholmur, Iceland. While exhibiting considerable interannual variability with concentrations of spectral power around periods of 2.1, 8, and 24 years [*Cook et al.*, 1998], the NAO has been in a generally positive phase since about 1970. A significant coherent relationship between the NAO and the North Atlantic sea surface temperature has been recently found at interannual and interdecadal timescales [*Higuchi et al.*, 1999]. The signature of the NAO is strongly regional and can be directly tied to variations in regional precipitation. Therefore the NAO index may be a relevant variable to the regional hydrology. For example, in a study on interannual variability of Canadian snow cover from 1915 to 1992 [*Brown and Goodison*, 1996], significant winter NAO-snow cover correlations were observed in Ontario and southern Quebec specifically in December. Another study [*Brown*, 1995] has shown that the influence of the NAO circulation pattern on winter snow cover was mainly confined to southern Canada.

[14] Another persistent climatic pattern that has to be considered in the Northern Hemisphere is the Pacific-North American (PNA) atmospheric teleconnection, which is defined as a measure of atmospheric response to a warm sea surface temperature (SST) anomaly in the central equatorial Pacific [*Wallace and Gutzler*, 1981]. The PNA has been found to be a dominant mode of variation in the middle latitudes during the winter months. It has been shown to be strongly related to precipitation and temperature within the same season in the western United States [*Redmond and Koch*, 1991]. Strongly positive and negative PNA indices are associated with warm events (El Niño) and cold events (La Niña), respectively, and with North American precipitation and temperature anomalies [*Yarnal and Diaz*, 1986]. It has been found that the pressure anomalies associated with the different phases of the PNA alter the normal upper atmospheric patterns, thus affecting temperature and precipitation patterns over various regions of North America [*Shabbar et al.*, 1997a].

[15] Station-based indices are now criticized as nonoptimal representations of the time-dependent behavior of their own associated spatial patterns [*Wallace*, 2000]. For example, rather than using a prescribed station-based NAO index, one may use the leading natural mode of variability as determined from principal component analysis of the hemispheric or global SLP field, based on observations or model control runs. It is noteworthy that there is no guarantee that the computed patterns represent real physical/dynamical modes of the climate system [*Hurrell et al.*, 2003]. Indeed, principal component analysis can reveal only orthogonal patterns. These issues (station-based versus derived leading components) are in the center of recent debate [*Wallace*, 2000; *Ambaum et al.*, 2001]. Therefore, in this study, two types of climatic patterns are considered. The Northern Hemisphere Annular Mode (NAM), originally called the Arctic Oscillation, is the first principal component of the Northern Hemisphere (20°–90°N) winter SLP field [*Thompson and Wallace*, 1998, 2000]. The NAM is shown to exert a strong influence on wintertime climate throughout middle- and high-latitude continental regions, affecting not only the mean conditions, but also the day-to-day variability associated with storm intensity and the occurrence of high-latitude blocking [*Thomson and Wallace*, 2001]. It explains 23% of the extended winter mean (December–March)

Table 1. Canadian Reference Hydrometric Basin Network (RHBN) Gauging Stations Used in the Wavelet Analysis

Region	Station Number	Latitude	Longitude	Drainage Area, km^2	Ecozone
			Eastern Canada		
1	02ZM006	47.6350	52.8372	3.63	Boreal Shield
1	02ZK001	47.2247	53.5683	285	Boreal Shield
1	02YR001	48.8078	54.2244	275	Boreal Shield
1	02ZH001	47.9469	54.2856	764	Boreal Shield
1	02YQ001	49.0153	54.8536	4400	Boreal Shield
1	02ZG001	47.2139	55.3292	205	Boreal Shield
1	02ZF001	47.7467	55.4417	1170	Boreal Shield
1	02YC001	50.6075	57.1511	624	Boreal Shield
1	02YL001	49.2406	57.3625	2110	Boreal Shield
1	02ZB001	47.6139	59.0092	205	Boreal Shield
1	02VC001	50.3078	63.6225	13000	Boreal Shield
2	01FB001	46.3694	60.9767	368	Atlantic Maritime
2	01FB003	46.2233	61.1367	357	Atlantic Maritime
2	01EO001	45.1733	61.9817	1350	Atlantic Maritime
2	01DG003	44.8517	63.6650	96.9	Atlantic Maritime
2	01CA003	46.7442	64.1856	46.8	Atlantic Maritime
2	01EF001	44.4467	64.5917	1250	Atlantic Maritime
2	01BU002	45.9436	65.1703	391	Atlantic Maritime
2	01AP002	46.0719	65.3667	668	Atlantic Maritime
2	01EC001	43.8383	65.3700	495	Atlantic Maritime
2	01AP004	45.7019	65.6014	1100	Atlantic Maritime
2	01BO001	46.7361	65.8267	5050	Atlantic Maritime
2	01BQ001	47.0947	65.8372	948	Atlantic Maritime
2	01BP001	46.9358	65.9072	1340	Atlantic Maritime
2	01AQ001	45.1700	66.4667	239	Atlantic Maritime
2	01BE001	47.8317	66.8817	2270	Atlantic Maritime
2	01AK001	45.945	67.3222	234	Atlantic Maritime
2	01BC001	47.6667	67.4842	3160	Atlantic Maritime
2	01AD002	47.2569	68.5931	14700	Atlantic Maritime
2	01AD003	47.2069	68.9569	1350	Atlantic Maritime
3	02PJ007	46.6592	71.2886	709	Mixedwood Plain
3	02OE027	45.4672	71.6553	642	Mixedwood Plain
3	02RD002	48.8994	72.2117	9320	Boreal Shield
3	02NF003	46.6858	73.9142	1390	Boreal Shield
3	02LB007	44.8422	75.5439	246	Mixedwood Plain
3	02KB001	45.8881	77.3083	4120	Boreal Shield
3	02HL004	44.5494	77.3292	712	Boreal Shield
3	02EC002	44.7128	79.2817	1520	Boreal Shield
3	02GA010	43.1906	80.4547	1030	Mixedwood Plain
3	02FB007	44.5225	80.9308	181	Mixedwood Plain
3	02FC001	44.4564	81.3267	3960	Mixedwood Plain
4	04NA001	48.6006	78.1094	3680	Boreal Shield
4	04LJ001	49.6167	83.2633	8940	Boreal Shield
4	04JC002	49.7789	84.5300	2410	Boreal Shield
4	02EA005	45.6694	79.3786	321	Boreal Shield
4	02AB008	48.3822	89.3078	187	Boreal Shield
4	02AA001	48.0122	89.6161	1550	Boreal Shield
			Central Canada		
5	05PB014	48.8500	92.7250	4870	Boreal Shield
5	06GD001	58.8917	96.2753	48100	Taiga Shield
6	05LH005	51.8528	99.5472	55000	Boreal Plain
			Western Canada		
7	08NF001	50.8861	116.0431	420	Montaine Cordillera
7	08NB005	51.4833	117.1792	9710	Montaine Cordillera
7	08NE087	49.4250	118.0417	80.5	Montaine Cordillera
7	08NE077	49.9075	118.1253	201	Montaine Cordillera
7	08LD001	50.9383	119.6544	3080	Montaine Cordillera
7	08LA001	51.6556	120.0653	10200	Montaine Cordillera
7	08NL007	49.4597	120.5019	1850	Montaine Cordillera
7	08MH016	49.0839	121.4567	329	Pacific Maritime
7	08KH006	52.8436	122.2236	11500	Montaine Cordillera
7	08MG005	50.3356	122.7994	2160	Pacific Maritime
7	08JE001	54.4181	124.2750	14600	Montaine Cordillera
7	08JB002	54.0092	125.0050	3600	Montaine Cordillera
8	08MH006	49.2428	122.5783	37.3	Pacific Maritime
8	08GA010	49.3958	123.1444	172	Pacific Maritime
8	08HA003	48.7275	123.6697	209	Pacific Maritime
8	08HA001	48.8792	123.7019	355	Pacific Maritime
8	08HB008	49.2897	124.9103	347	Pacific Maritime
8	08HE006	50.0144	126.8425	181	Pacific Maritime
9	07FB001	55.7200	121.2078	12100	Montaine Cordillera
9	10CD001	58.7883	122.6592	20300	Taiga Plain, Boreal Cordillera
9	10CB001	57.2342	122.6942	2160	Taiga Plain, Boreal Cordillera
9	10BE004	58.8556	125.3806	2570	Boreal Cordillera
9	08CE001	57.9008	131.1544	29300	Boreal Cordillera
9	08CG001	56.7389	131.6736	9350	Montaine Cordillera
9	09AE003	59.9306	131.7678	3320	Boreal Cordillera
9	09BA001	61.9944	132.3778	7250	Boreal Cordillera
9	09AA006	59.5992	133.8133	6810	Boreal Cordillera
9	09AC001	60.8522	135.7392	6990	Boreal Cordillera
9	09BC001	62.8297	136.5806	49000	Boreal Cordillera

variance and is largely dominated by the NAO structure in the Atlantic sector [*Hurrell et al.*, 2003]. *Serreze et al.* [2000] consider the NAO as a major component of the NAM, with cold-season correlation of about 0.8. The NAM pattern, like the NAO, has been generally positive since the early 1970s.

[16] In addition to the NAO, PNA, and NAM indices, indicators of the El Niño-Southern Oscillation (ENSO) are also selected for this study. The ENSO phenomenon is characterized as a spreading of warm water off the coast of South America from the equatorial central Pacific to the eastern Pacific and is associated with climatic anomalies throughout the world. The ENSO index used in this study is the monthly mean equatorial Pacific sea surface temperatures (SST) anomalies over the Niño-3 region (5°N–5°S; 90°W–150°W) [*Rasmusson and Carpenter*, 1982]. For notational simplicity, ENSO3 will be used herein to denote the SST anomalies over that region. The influence of ENSO on streamflow is well documented [*Redmond and Koch*, 1991; *Kahya and Dracup*, 1993; *Dracup and Kahya*, 1994; *Eltahir*, 1996; *Kiem and Franks*, 2001], and subsequently the use of the ENSO-streamflow relationship for predictive purposes has been studied extensively in recent years [*Moss et al.*, 1994; *McKerchar et al.*, 1996; *Piechota et al.*, 1997, 1998; *Piechota and Dracup*, 1999; *Coulibaly et al.*, 2000; *Gutiérrez and Dracup*, 2001].

[17] It is noteworthy that some climatic indices are relatively interlinked over some time periods. As indicated previously, the NAM index is considered as a "sister of the NAO" [*Serreze et al.*, 2000]; PNA and ENSO3 are connected as documented previously; and a complex relationship has been recently shown between the NAO, ENSO, and PNA patterns [*Huang et al.*, 1998]. However, the dynamical relationship between climatic patterns remains controversial and warrants further research [*Diaz et al.*, 2001; *Hurrell et al.*, 2003]. Therefore the selected climatic patterns are used here as independent variables in order to assess the specific link between each climatic indictor and the Canadian streamflows.

3. Methods

[18] The decomposition of time series into time-frequency space permits the identification of the dominant modes of

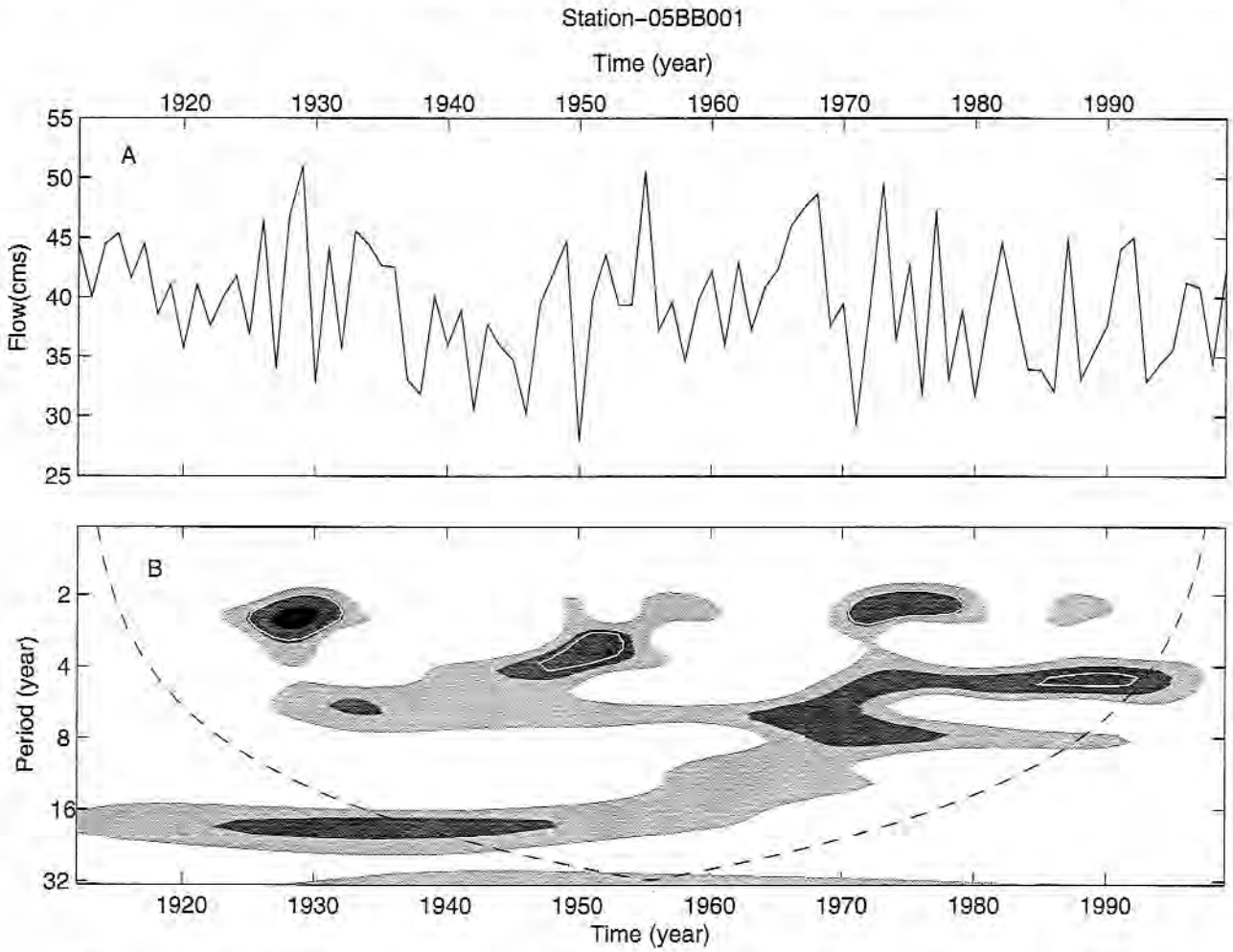

Figure 2. Bow River at Banff (station 05BB001). (a) Time series of mean annual streamflows. (b) Normalized local wavelet power spectrum of the streamflows using the Morlet wavelet. The shaded contours are at normalized variance of 1, 2, and 4. The dashed curve depicts the cone of influence beyond which the edge effects become important. The white contour lines enclose peaks of greater than 95% confidence for a red noise with a lag-1 coefficient α of 0.18.

variability and how these modes vary in time. This can be done by using either windowed Fourier transform or wavelet transform. However, a shortcoming of standard Fourier transform is that it does not provide an accurate time-frequency localization, nor does it perform well on irregularly spaced events or nonstationary signals [*Smith et al.*, 1998]. A major advantage of using the wavelet transform over the Fourier transform is that wavelet analysis is scale independent [*Kaiser*, 1994], and hence there is no need for a predetermined scale (or response interval), which would limit the frequency range. Continuous wavelet transform is more appropriate for geophysical and hydrological time series because of the wide range of possible dominant frequencies. Moreover, it is also an efficient method for analyzing nonstationary signals [*Daubechies*, 1990].

[19] The wavelet analysis method described herein is limited to the needs of the present study. Emphasis is given to useful practical details for applying the method for hydrological time series analysis. For a more detailed description of wavelet analysis in geophysics and hydrology, the readers are referred to other sources, such as *Torrence and Compo* [1998] and *Labat et al.* [2000]. The continuous wavelet transform of a discrete sequence of observations x_n is defined as the convolution of x_n with a scaled and translated wavelet $\psi(\eta)$ that depends on a nondimensional time parameter η,

$$W_n^X(s) = \sum_{n'=0}^{N-1} x_{n'} \psi^* \left[\frac{(n'-n)\delta t}{s} \right], \quad (1)$$

where n is the localized time index, s is the wavelet scale, δt is the sampling period, N is the number of points in the time series, and the asterisk indicates the complex conjugate. Since complex wavelets lead to complex continuous wavelet transform, the wavelet power spectrum, defined as $|W_n(s)|^2$, is a convenient description of the fluctuation of the variance at different frequencies. Further, when normalized by σ^{-2} (where σ^2 is the variance), it gives a measure of the power relative to white noise, since the expectation value for a white noise process is σ^2 at all n and s.

[20] Figure 2b illustrates the normalized local wavelet power spectrum of a typical streamflow time series

(Figure 2a) using the Morlet wavelet, a complex non-orthogonal wavelet consisting of a plane wave modulated by a Gaussian:

$$\psi_0(\eta) = \pi^{-0.25} e^{i\omega_0\eta} e^{-0.5\eta^2} \quad (2)$$

where ω_0 is the nondimensional frequency. The advantage of the Morlet wavelet over other candidates such as the Mexican hat wavelet resides in its good definition in the spectral-space. For $\omega_0 = 6$ (used here), the Morlet wavelet scale is almost identical to the corresponding Fourier period of the complex exponential, and the terms "scale" and "period" may conveniently be used synonymously [*Torrence and Compo*, 1998; *Torrence and Webster*, 1999]. Thus the left axis in Figure 2b is the equivalent Fourier period corresponding to the wavelet scale (hereinafter called the wavelet period), and the bottom axis is time (in years). The shaded contours are the normalized variance in excess of 1, 2, and 4. Features with variance larger than expected for a white noise process reveal that the interannual variability is organized in preferential bands of wavelet periods. These bands, 2–3, 3–6, 6–12, and beyond 12 years, have been reported by other investigators in precipitation and streamflow time series [*Rajagopalan and Lall*, 1998; *Coulibaly et al.*, 2000]. This suggests the choice of the scale-averaged wavelet power to further examine fluctuations in power over specific ranges of wavelet periods (bands). Scale-averaged wavelet power is defined as the weighted sum of the wavelet power spectrum over scales s_1 to s_2:

$$\bar{W}_n^2 = \frac{\delta j \delta t}{C_\delta} \sum_{j=j_1}^{j_2} \frac{|W_n(s_j)|^2}{s_j}. \quad (3)$$

where δj is a factor that dictates the scale resolution (chosen as 0.1), and C_δ is a reconstruction factor specific to each wavelet form; $C_\delta = 0.776$ for the Morlet. This approach also allows increasing the degree of freedom of the power estimators. In Figure 2, the dashed curve depicts the cone of influence of the wavelet analysis [*Torrence and Compo*, 1998]. Any peaks outside the cone of influence have presumably been reduced in magnitude due to the zero padding necessary to deal with finite length observations. For example, it is possible that activity around a period of 16 years in Figure 2 (see, for example, *Hu et al.* [1998] for an exploration of such periods) carries on at both ends of the time series instead of diminishing, as illustrated. For the span of the available streamflow data, it is thus not reasonable to consider wavelet periods much beyond 12 years. Three bands of wavelet periods are examined in greater detail: 2–3, 3–6, and 6–12.

[21] Finally, the power spectrum produced for a given time series is the product of the natural process involved and noise. The contour lines in Figure 2 identify peaks of greater than 95% confidence for a red noise process with a lag-1 coefficient α of 0.18 following the Monte Carlo analysis of *Torrence and Compo* [1998] based on the univariate lag-1 autoregressive process. It must not be presumed that regions of the power spectrum out of these 95% confidence level areas are the product of noise only. The natural process is also present in these regions but influences the power spectrum to a lesser extent. The coefficient α is series specific and is estimated for each series.

4. Wavelet Analysis Results

4.1. Eastern Canada

[22] The scale-average wavelet power represents the average variance ($\bar{\sigma}^2$) over a range of scales (or a certain band). It provides an efficient way to examine the fluctuations in power over a desired band. By averaging the wavelet power spectra at multiple locations, one can simultaneously assess the spatial and temporal variability of the streamflow data. Figure 3a shows a power Hovmöller [*Torrence and Compo*, 1998], a time-longitude diagram of the normalized scale-averaged wavelet power of the eastern Canada streamflows in the 2–3 year band at the longitude location of each hydrometric station. At each longitude, the wavelet power spectrum is computed using the Morlet wavelet, and the scale-averaged wavelet power over the 2–3 year band is calculated from equation (3). Then all the scale-averaged wavelet power time series (equation (3)) are combined in a two-dimensional contour plot, with 95% confidence level computed using the lag-1 autocorrelation at each site. To allow the juxtaposition of streamflow from watersheds of different sizes, each scale-averaged series is normalized by σ^{-2} of the original series. The zonal-average of the power Hovmöller (Figure 3b) gives a measure of the average 2–3 year variance of the streamflows over eastern Canada. It typically shows the temporal fluctuations of the streamflows over the entire area. For example, activities in the 2–3 year band account for up to 45% of the average variance (0.45 $\bar{\sigma}^2$) between 1978 and 1982, with a second moderate peak (0.30 $\bar{\sigma}^2$) between 1955 and 1960. Figure 3c shows the time-averaged 2–3 year power as function of longitude. The longitudinal distribution of the power spectra (Figures 3a and 3c) reveals three local patterns: a low activity zone at 50°–60°W, an intense activity zone at 60°–77.5°W, and a moderate activity region at 77.5°–90°W, corresponding (see Table 1) to region 1 (Boreal Shield: Newfoundland-Labrador and Northern Quebec), region 2 (Atlantic Maritime: Nova Scotia, New Brunswick, and Prince Edward Island) and part of region 3 (Mixedwood plain: Southern Quebec and upper St. Lawrence/Lake Ontario); and region 4 (Boreal Shield: Ontario) and part of region 5 (Boreal/Taiga Shield: western Quebec), respectively. This may suggest that the division of flow stations into climatic regions can be refined by considering the space-time variability of mean annual flows. In general, the eastern Canada streamflows are characterized by locally intense activities in the 2–3 year band with moderate peaks in 1945 and 1955, and stronger peaks in the 1980s. There is no significant structure in that band prior to the 1940s.

[23] Figure 4 illustrates the power Hovmöller for the 3–6 year band of eastern Canada streamflows. The general level of activity is slightly similar to the preceding band (2–3 year), but with different timing. The activity in the 3–6 year band accounts for up to 0.5 $\bar{\sigma}^2$ around 1930s, with a second peak (0.4 $\bar{\sigma}^2$) between 1950 and the late 1960s (Figure 4e). There is an organized activity in that band since the 1930s, with fluctuations differing as a function of longitude until the 1990s. Here again, the longitudinal distribution of the power spectra (Figures 4d and 4f)

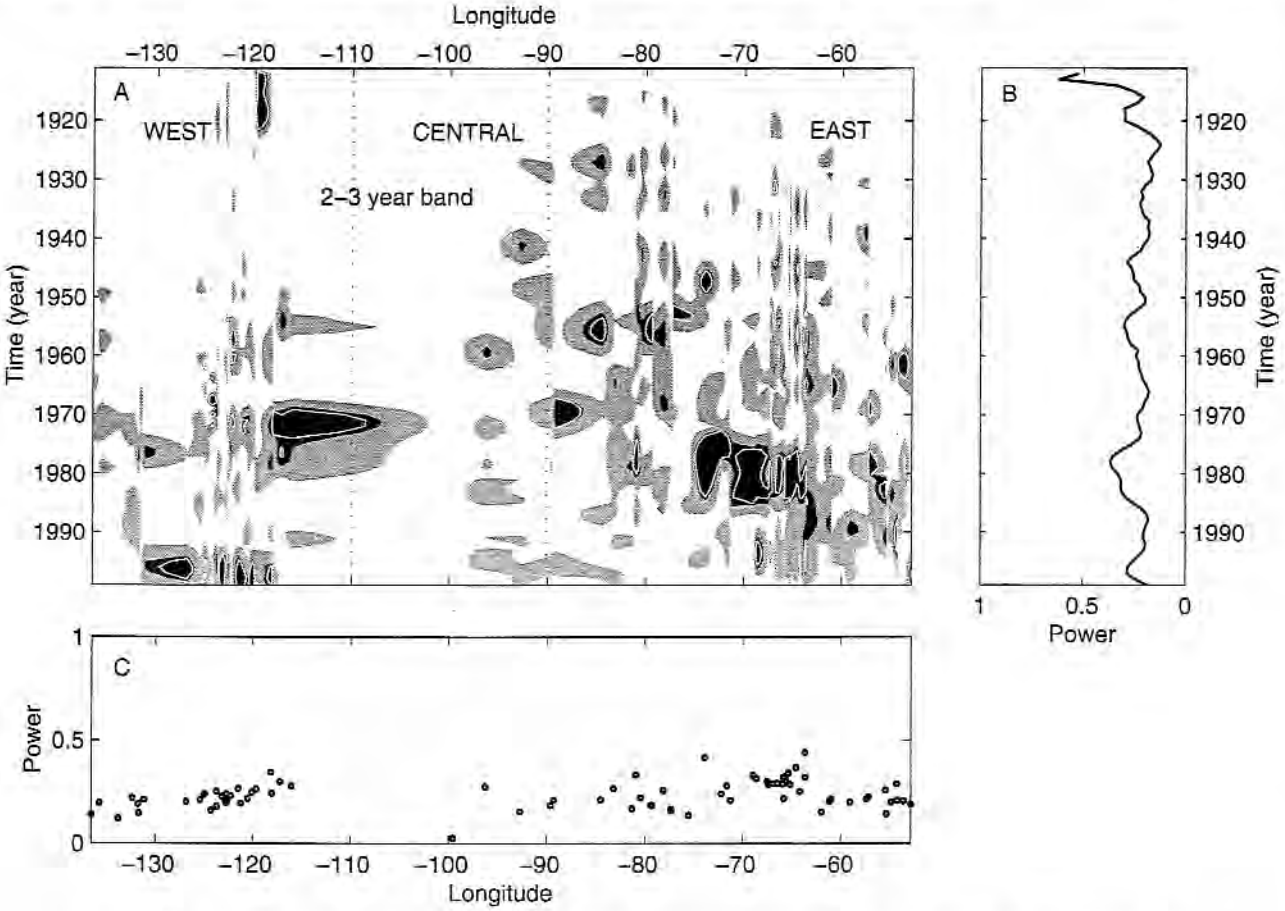

Figure 3. Time-longitude diagrams of the Canadian annual flows in the 2–3 year band. (a) Hovmöller plot of the normalized scale-averaged wavelet power. The shaded contours are at normalized power of 0.2, 0.5, and 1. The white contour lines enclose peaks of greater than 95% confidence computed using the lag-1 autocorrelation at each site. (b) Space-average of the power Hovmöller. (c) Time-average of the power Hovmöller. Each circle corresponds to a flow station location.

suggests three regions with low, high, and moderate activity, thus confirming that finer regionalization of the flow stations may be obtained by assessing the low-frequency fluctuations of mean annual streamflows. The timing of the zonal-scale fluctuations in the 2–3 year band (Figure 3b) and the 3–6 year band (Figure 4e) is surprisingly opposite, suggesting that these structures are driven by different climatic phenomena or a combination of climatic patterns. Figure 5 presents the power Hovmöller for the 6–12 year band of eastern Canada streamflows. There is only one significant structure (or peak) in that band, accounting for about 0.25 $\bar{\sigma}^2$ around the 1930s. There has been no organized activity in the 6–12 year band for the last 60 years. It should be noted that caution must be exercised in interpreting the results for the 6–12 year band since many of the stations have record lengths that are shorter than would be desired for this type of analysis.

4.2. Central Canada

[24] The limited number of stations with longer records available in central Canada suggests that the wavelet analysis results presented herein are not representative of the entire region and must be interpreted with caution. Figures 3–5 show the power Hovmöller for the 2–3, 3–6, and 6–12 year bands of central Canada streamflows. In the 2–3 year band, there is a single activity accounting for up to 0.55 around the 1940s, while in the 3–6 year band, there are two intense activities corresponding to a strong peak (0.65 $\bar{\sigma}^2$) in the 1930s and a second strong peak (0.60 $\bar{\sigma}^2$) between 1980 and 1990. In the 6–12 year band, a moderate activity accounts for about 0.50 $\bar{\sigma}^2$ around the 1930s.

[25] Although the longitudinal distribution of the power spectra is questionable because of the limited number of stations, the zonal average still provides a good measure of the temporal fluctuations of the streamflow. In general, there has been no organized activity in the 2–3 and 6–12 year bands in the last 50 years. The 3–6 year band is characterized by a strong activity between 1920 and 1930 followed by a no-activity period (1940–1970), and a second strong activity between 1980 and 1990. Those temporal fluctuations are essentially reflected by one site (station 06GD001 at 96.27°W). Additional streamflow records will be necessary to further assess the spatial and temporal variability of streamflows in central Canada.

4.3. Western Canada

[26] In this analysis, the western Canada streamflows cover regions 7, 8, and 9 (see Table 1) with a total of 29 stations, thus allowing a better space-time variability analysis of streamflows as compared to the central part of

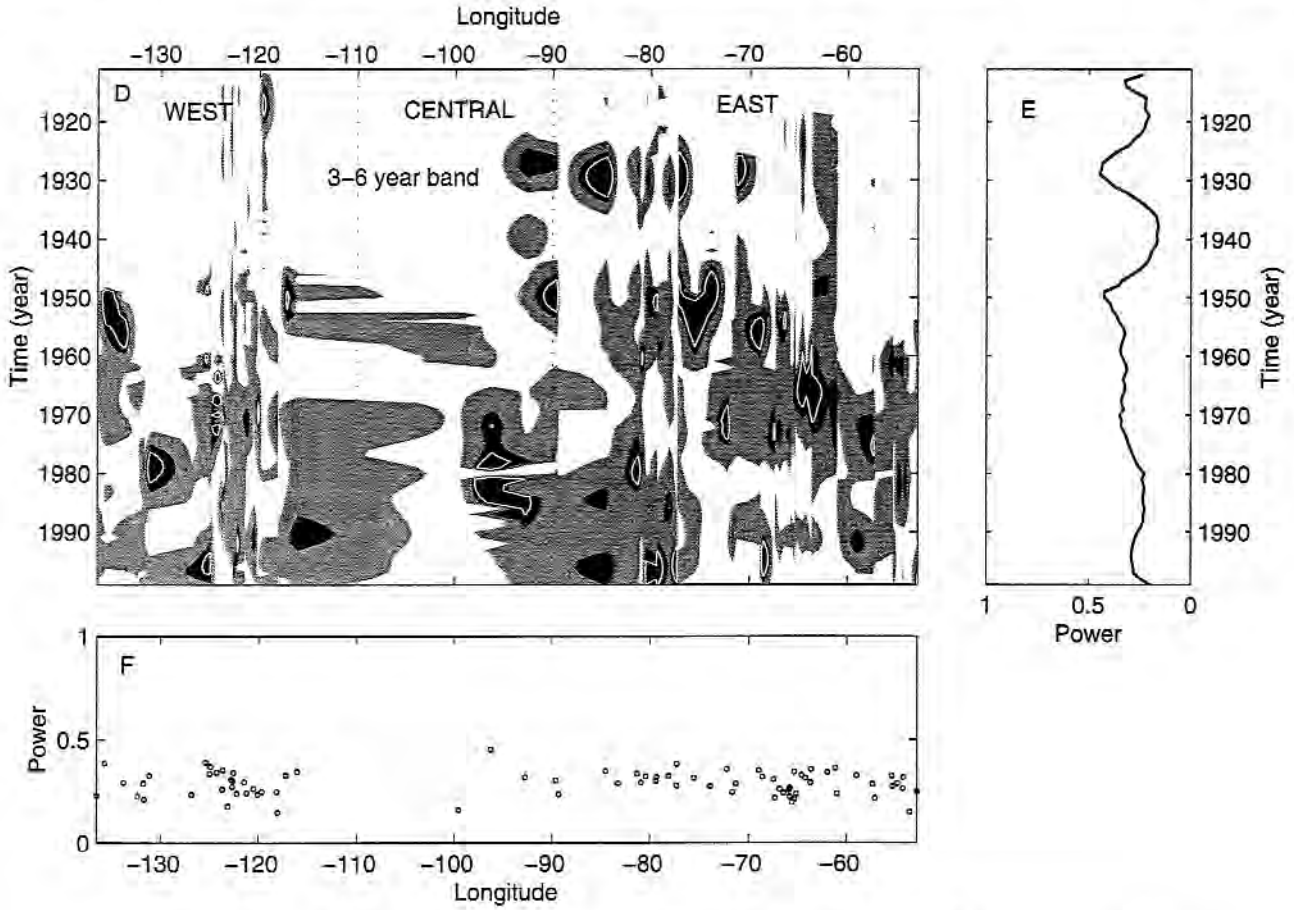

Figure 4. Time-longitude diagrams of the annual flows in the 3–6 year band. Features are identical to Figure 3.

Canada. Figure 3 presents the power Hovmöller for the 2–3 year band of western Canada streamflows. The strongest activity in this band is in the 1920s, accounting for up to 0.90 $\bar{\sigma}^2$ (Figure 3b), with a second peak (0.40 $\bar{\sigma}^2$) between 1970 and 1980, and a third peak (0.45 $\bar{\sigma}^2$) in 1998. There is no organized activity in that band between 1925 and 1965. Here the longitudinal distribution of the power spectra (Figures 3a and 3c) suggests three distinct activity zones: an intense activity zone at 116–121W, a moderate activity region at 121–129W, and a no activity zone at 129–136.5W – corresponding approximately (see Table 1) to region 7 (Montaine Cordillera – British Columbia), region 8 (Pacific Maritime – British Columbia), and region 9 (Boreal Cordillera – British Columbia/Yukon Territories) respectively. It appears that some flow stations (actually in region 7 or 9) can belong to neighboring region 8 – suggesting that a refinement of the station division may be possible based on the wavelet analysis of the annual sreamflows. Figure 4 illustrates the power Hovmöller for the 3–6 year band of Western Canada streamflows. The general level of activity is slightly similar to the preceding band (2–3 year), but with different longitudinal distribution and slightly similar timing except for year 1950. The activity in the 3–6 year band is characterized by three moderate peaks (in 1920, 1950, 1970) and a lower peak in 1998 (Figure 4e). The longitudinal distribution of the power spectra (Figure 4d) confirms the three distinct activity zones (116–121W, 121–129W, and 129–136.5W) but with different level of intensity as compared to the activity level in the 2–3 year band. The Boreal Cordillera (region 9) seems dominated by the 3–6 year activity while the Montaine Cordillera (region 7) is more strongly affected by the 2–3 year band activity. Only the Pacific Maritime appears equally affected by both the 2–3 year and the 3–6 year activity. There is no organized structure in the 6–12 year band as indicated by its power Hovmöller (Figure 5). The overall level of activity in that band accounts for only 0.15 $\bar{\sigma}^2$, and thus it consists essentially of white noise. Again, care must be taken in interpreting these results due to the presence of stations with short record lengths.

4.4. Power Hovmöller of Canadian Streamflows

[27] To simultaneously assess the spatial and temporal variability of the annual streamflows throughout Canada, the time-longitude diagrams of the annual flows (from western to eastern Canada), Figures 3–5 are discussed. It is noteworthy that even an apparently small feature in these figures represents a significant activity. The smaller structure sizes are due to scale reduction to allow juxtaposition of all the 79 stations and to provide a complete overview of the spatial and temporal variability of the streamflows (from west to east). It appears from Figure 3 that organized activity in the 2–3 year band starts after the 1940s except for western Canada, where a strong activity is observed in the 1920s.

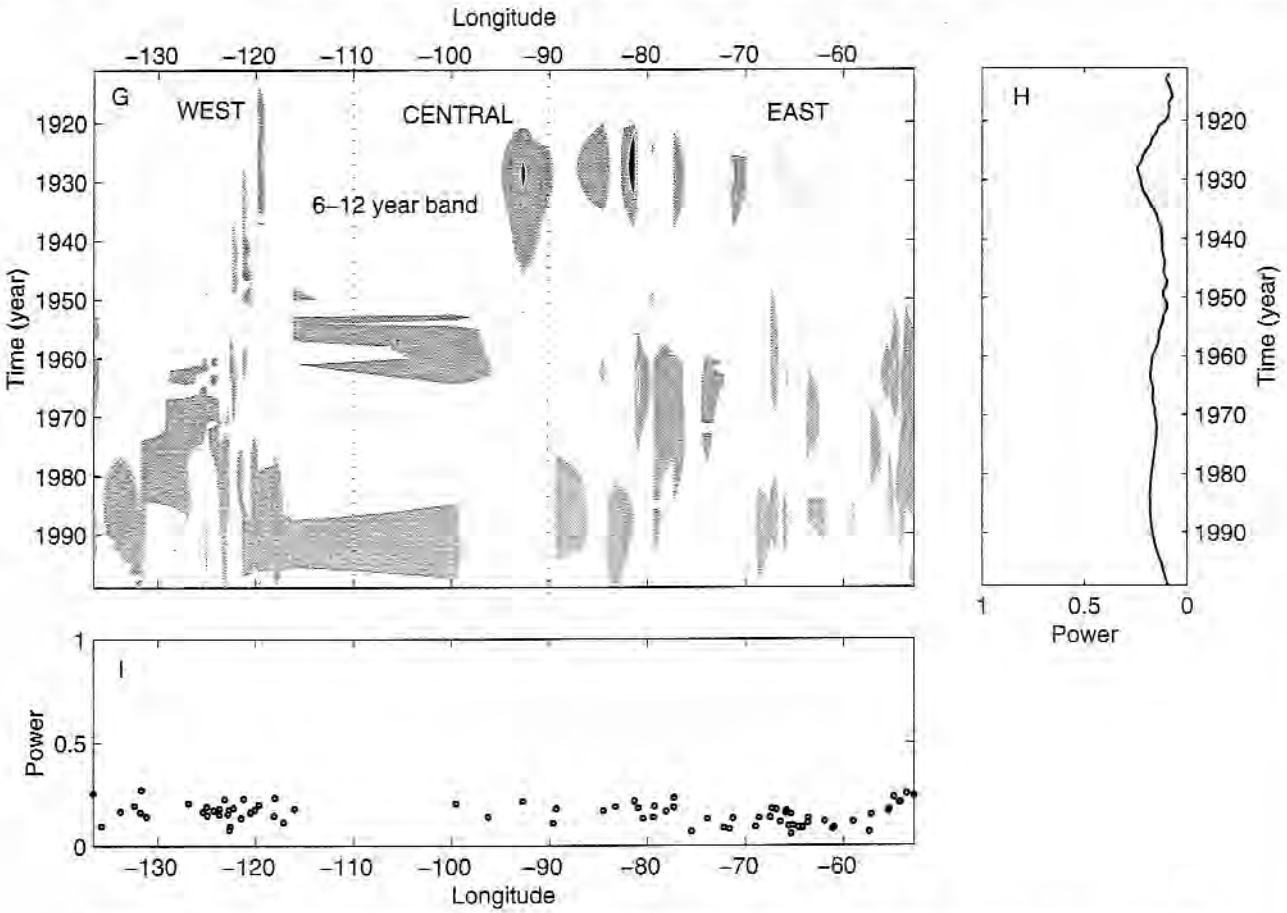

Figure 5. Time-longitude diagrams of the annual flows in the 6–12 year band. Features are identical to Figure 3.

Moderate activity is revealed between 1950 and 1960, and major (intense) activity is revealed between 1970 and 1990. Conversely, in the 3–6 year band (Figure 4), the major activity is observed between 1950 and 1970 and moderate activity between 1920 and 1930 and between 1980 and 1990. However, in both cases, years 1950 and 1970 can be seen as particular points in the streamflow variability level. A moderate 6–12 year activity is revealed around the 1930s only in the eastern and central Canada streamflows (Figure 5). There has been no organized activity in the 6–12 year band since 1940. In general, the Canadian streamflows appear essentially dominated by the 2–3 and 3–6 year activity. Therefore only the 2–3 and 3–6 year bands are considered herein for the streamflow-climatic pattern study.

4.5. Streamflow and Climatic Patterns

[28] To examine the dynamic relationship between the streamflow and the selected climatic indices, the dominant structures of the interannual variability in the streamflows revealed by the power Hovmöller plots are exploited. Principal component (PC) analysis is used to construct three streamflow time series corresponding to western, central, and eastern Canada streamflows. The west PC series are obtained from the 29 stations located between 110°W and 140°W, the central PC series are constructed from the three stations (between 90°W and 100°W), and the east PC series are obtained for the 47 stations between 40°W and 90°W (see Figure 1). In each case, the leading PC selected (Figure 6) explains at least 70% of the total variance. Specifically, the west leading PC explains 80% of the total variance, while the central and the east PCs explain 95% and 75% of the total variance, respectively. The PC series (Figure 6) reveals three possible time periods in the streamflow variability: one in 1911–1950, a second in 1950–1970, and third in 1970–1999, each characterized by a different trend and level of variability. This raises an interest in investigating further the streamflow power during these three periods. The PC series as shown in Figures 7 and 8 do preserve the main interannual features revealed in the power Hovmöller plots for the 2–3 and 3–6 year bands. Figure 7 shows the 2–3 year scale-average power spectra for the PC streamflow series and the teleconnection patterns considered. Figure 7 reveals a positive correlation between the west streamflow power and the ENSO3 activity particularly after 1950, while a negative correlation with the PNA activity is shown since 1950. Note that the PNA series are available only from 1950, while the others are available for the entire period (1911–1999) considered. To further substantiate the results in Figure 7, correlation analysis results for the 2–3 year band are presented in Table 2, for data before and after 1950, data before and after 1970, and for all available data (1911–1999). Considering the complete data set, the western streamflow activity in the 2–3 year band is essentially depicted by the ENSO3, with a correlation value of 0.52. The west streamflow power is also nega-

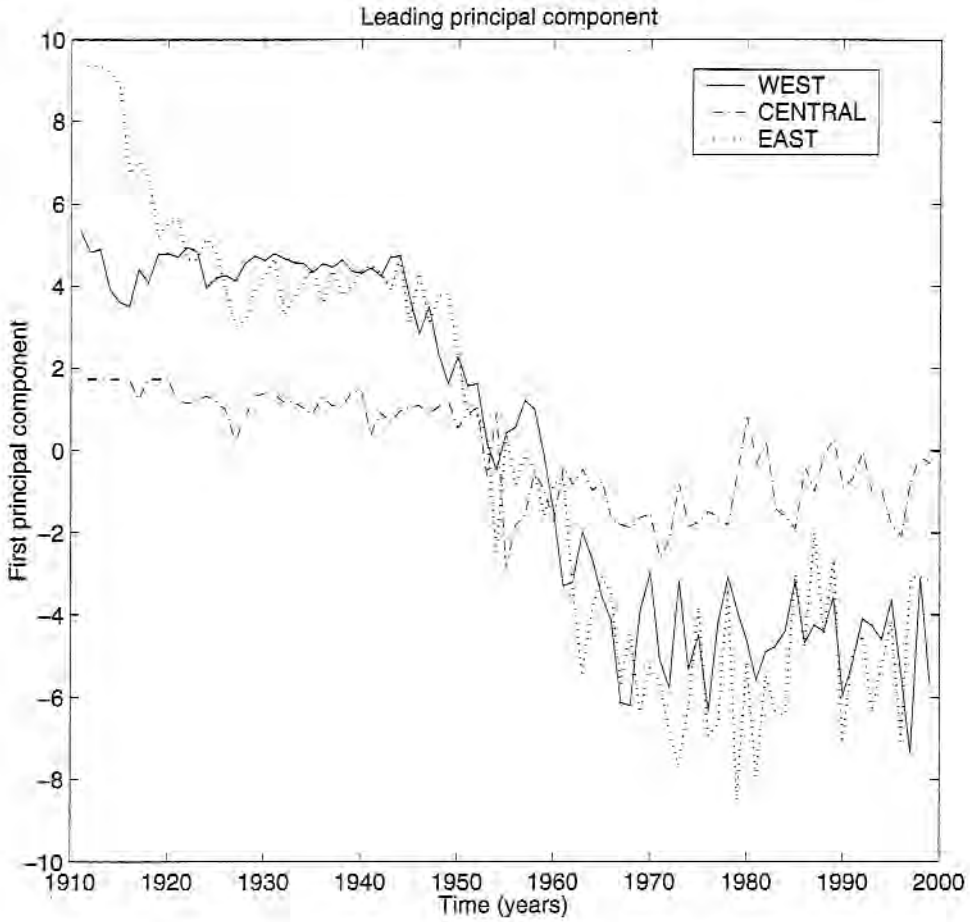

Figure 6. Time series of the flow leading principal component: west, central, east.

tively correlated to the PNA (−0.47) for the period 1970–1999, while there is no correlation with the NAO and the NAM.

[29] The central streamflow power is negatively correlated to ENSO3 (−0.50) and PNA (−0.55) during 1950–1999 and 1950–1970, respectively. Again, the NAO and the NAM are not correlated to central streamflow power. Conversely, the eastern streamflow power is positively correlated to NAM prior to 1950 (0.53) and negatively correlated with NAO afterward (−0.64), confirming that these "twin patterns" do not have the same temporal distribution of power as shown in Figure 7. East is also correlated to ENSO3 (−0.48) only after 1970, but more correlated to the PNA (0.66) during 1950–1999. Since 1950, the eastern streamflow activity in the 2–3 year band is depicted mainly by the PNA and the NAO, while the central and western streamflow activities are mostly related to the ENSO3 and the PNA. Considering all the data analyzed for the entire period (1911–1999), the Canadian streamflow activity in the 2–3 year band is correlated to the PNA (0.48) during 1950–1999, but before 1950 it is mainly correlated to the NAM (0.62), but with no correlation to the NAO. Conversely, after 1970, the Canadian streamflow power is negatively correlated to the NAO (−0.55), while there is no correlation to the NAM for that period. This may indicate that even though the NAO and the NAM are two representations of the same phenomenon [*Wallace*, 2000], they are not identical. It has been shown that the NAM index is more strongly coupled to Eurasian winter surface air temperature than the NAO index [*Thompson and Wallace*, 1998], suggesting that NAM and NAO can have different impacts in a specific region.

[30] Similar analysis is performed for the 3–6 year band (Figure 8 and Table 3). The higher level of activity in the 3–6 year band discussed earlier is reflected in general by stronger correlations with the teleconnection patterns. Here again, the west is correlated to the ENSO3 (−0.48), but also to the NAO (−0.69), and the PNA (−0.59) during 1950–1999. The increasing level of activity in the west (since 1950) is likely related to PNA as indicated by the increasingly strong correlations since 1950. A striking element of the correlation results here is that after 1970, the west is negatively correlated to all the climatic patterns selected, while before 1970, it is correlated only to the PNA. Similarly, after 1950, the west is negatively correlated to ENSO3 and NAO, while there was only a positive correlation to NAO prior to 1950. From these results, one can argue that years 1950 and 1970 may represent changing points in west streamflow activity, and this appears consistent with the recent study of *Chen and Rao* [2002], who tested the stationarity of midwestern United States hydrologic time series using segmentation analysis and identified change points between 1960 and 1970. Furthermore, the 1970 change point may also be related to the enhancement of the power in the 3–6 year band for both the NAO and the PNA since 1970 (Figure 8), suggesting that change point in

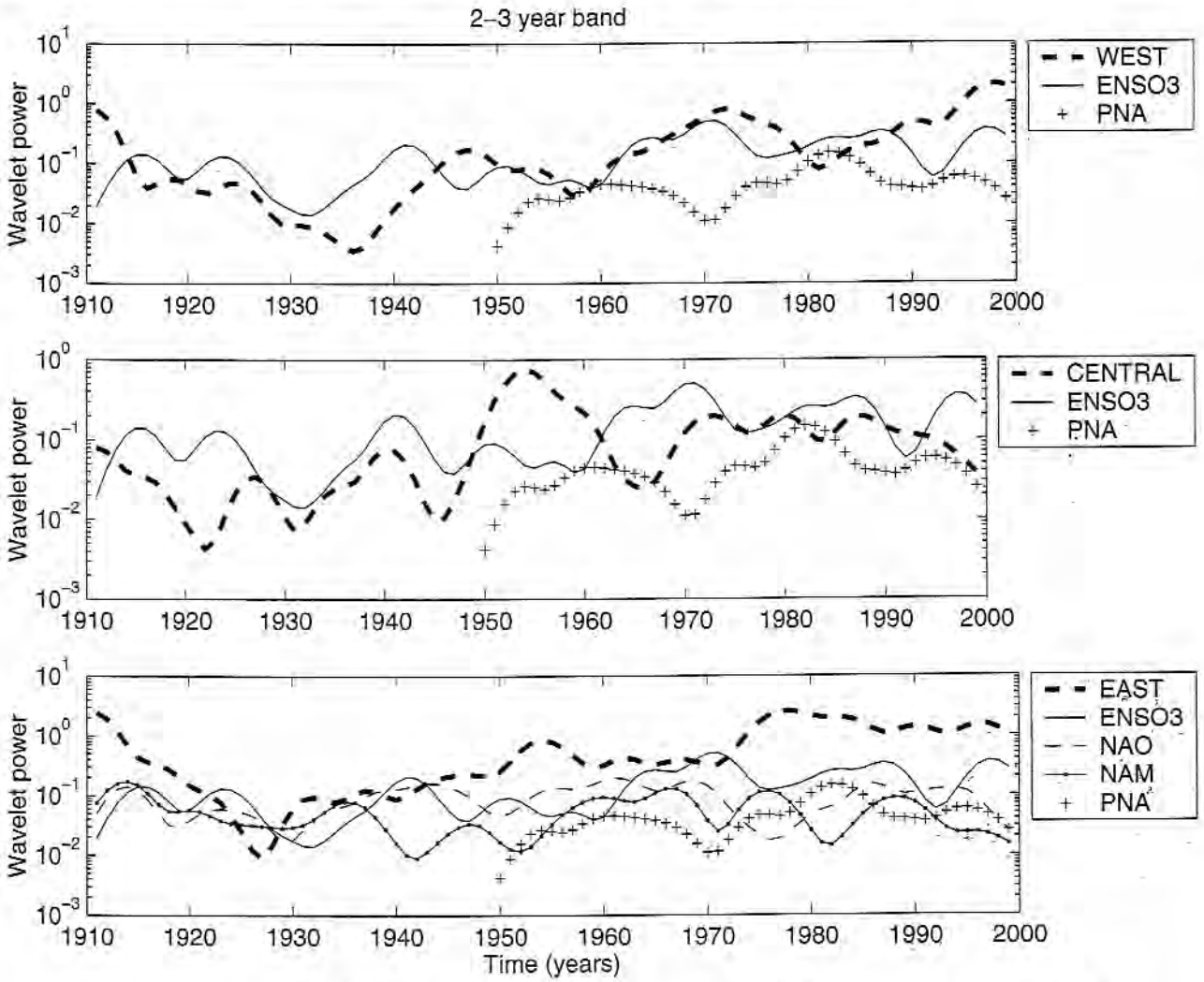

Figure 7. Time series of the scale-averaged wavelet power for the 2–3 year band: west, central, east, and selected climatic indices.

streamflow variability may not only reflect sudden changes in intensity of climatic patterns, as shown by the teleconnection indices, but also can be attributed to modifications in the dominant atmospheric circulation modes that affect a specific region. This obviously requires further investigation to be illustrated. Still, in the 3–6 year band, the central streamflow power is highly correlated to the PNA (0.75) prior to 1970 and moderately correlated to the NAO (−0.46) after 1970. Here ENSO3 and NAM are not correlated to the central streamflow power. The eastern streamflow activity is correlated to ENSO3 (−0.66) and NAO (−0.73) since 1950, with stronger correlations (−0.70 and −0.79, respectively) after 1970. East is also strongly correlated to the PNA (−0.84) prior to 1970 and less correlated afterward. Here again, there is a significant enhancement in the intensity level of the teleconnection indices (ENSO3, NAO) after 1950 and 1970, respectively, suggesting two possible change points: a first one in 1950 and a second one in 1970. This is consistent with previous studies in eastern Canada. *Shabbar et al.* [1997b] identified a detectable cooling in winter surface temperature data from 12 stations in coastal eastern Canada and western Greenland since 1970 that was linked to an enhancement of the negative phase of the NAO index and of the positive phase of the PNA. *Perreault et al.* [2000] used a Bayesian method to identify a change point in annual reservoir inflows for the Outaouais basin in eastern Canada. They reported a change point around 1979 with approximately 12 years of standard deviation. Although the change point in 1950 suggested by the present results may require further investigation, it is clear from the present analysis that the east and the west 3–6 year bands are negatively correlated to the ENSO3 and NAO since 1950, which was not the case prior to that change point. Similar findings substantiate the 1970 change point in the west and the east (see Table 3). The low activity level in central Canada streamflows is associated with the limited data in this area, as discussed earlier. Additional streamflow records will be needed to assess whether the 1950 and 1970 change points appear in that region.

[31] In general, considering the entire data set during 1911–1999, the Canadian streamflow activity in the 3–6 year band is depicted mainly by the NAO (−0.61), the ENSO3 (−0.58), and the PNA (−0.53). Surprisingly, there is no significant correlation with NAM since 1950. In both

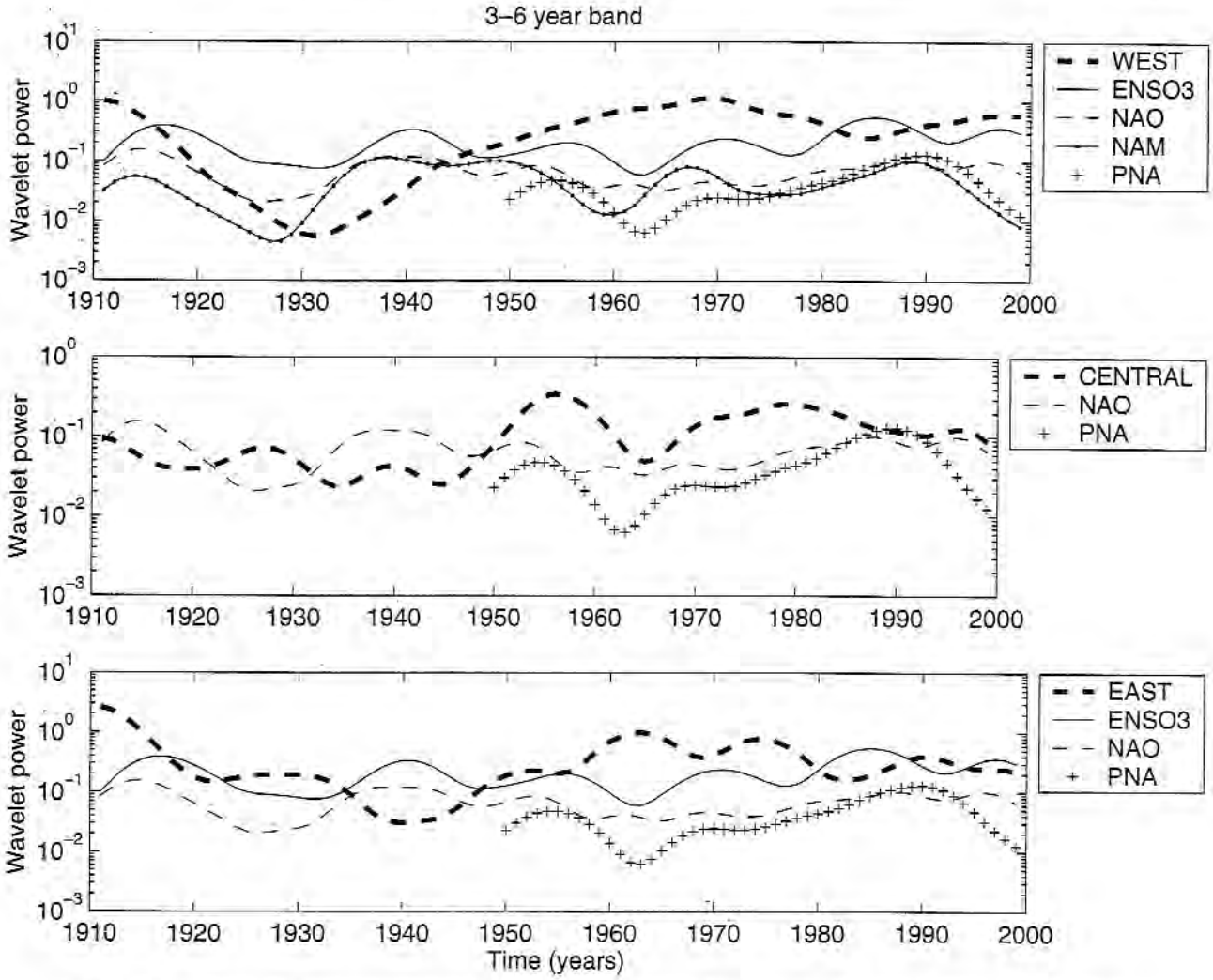

Figure 8. Time series of the scale-averaged wavelet power for the 3–6 year band: west, central, east, and selected climatic indices.

the 2–3 and 3–6 year bands, the Canadian streamflows are depicted mainly by the PNA and the NAO and by the ENSO especially in the 3–6 year band, which is consistent with the ENSO cycle.

5. Discussion

[32] The wavelet analysis results presented in the previous section reveal clear temporal patterns which can be used to refine streamflow regionalization over the Canadian Reference Hydrometric Basin Network (RHBN). The main characteristic timescales (2–3 and 3–6 year periods) of the annual streamflows revealed by the global wavelet spectra along with the strong climate related correlations identified provide qualitative information that is essential to any attempt to investigate the effects of climate change on streamflows. For example, it is clear from Table 2 that since 1950, the eastern streamflow activity in the 2–3 year band is mostly related to the PNA and NAO, while the central and western streamflows are mainly dominated by the ENSO3 and the PNA. Such streamflow-climate relationship can also be used to improve long-range forecasting, which is an essential part of the development of optimal reservoir planning and operation policies for power generation, water supply, and flood control. For example, the use of the ENSO-streamflow relationship for predictive purposes has shown promising results in recent studies [*Piechota et al.*, 1998; *Coulibaly et al.*, 2000; *Gutiérrez and Dracup*, 2001]. However, further analysis of the climate-streamflow relationship may be required and should include other methods such as cross-wavelet analysis to highlight the temporal variation in the relationship between streamflows and climate indicators. The integration of the observed temporal structures and the related climatic patterns into streamflow simulation would require a suitable hydrologic model which can take into account all the observed dynamic components of the streamflow.

6. Conclusions

[33] The continuous wavelet transform offers an effective tool for both describing interannual features and quantifying the temporal variability of annual streamflows. Scale-averaged wavelet spectra permit us to simultaneously assess the interannual and spatial variability in 79 streamflow time series. The span of the available streamflow records, 1911–

1999, allows depicting the interannual variance (or activity) for periods up to 12 years, and thus three periods, namely, 2–3, 3–6, and 6–12 year bands, are investigated. It is shown that the Canadian streamflows are essentially dominated by the 2–3 and 3–6 year activity with net differences between the timing and the intensity of the interannual variability in western, central, and eastern Canada. The 6–12 year band activity is dominated by white noise in all the regions since 1950. Correlation analysis between streamflow activity and climatic pattern power in both the 2–3 and 3–6 year bands revealed two major change points, namely, 1950 and 1970 in western and eastern streamflows, while it is concluded that central Canada requires additional streamflow records to assess similar change points. In the 2–3 year band, western and central streamflow activity is essentially depicted by the ENSO3 and the PNA since 1950, while the eastern streamflow activity is highly correlated to the NAO and PNA. In general, the Canadian streamflow activity in the 2–3 year band is depicted by the NAM prior to 1950, the PNA since 1950, and the NAO since 1970.

[34] Stronger correlations with the teleconnection patterns are observed in the 3–6 year band. The most striking elements in the 3–6 year band are that since 1970, the west is strongly negatively correlated to all the climatic patterns, while before 1970, it was correlated only to the PNA. Similarly, since 1950 the west and east are highly negatively correlated with the ENSO3 and NAO, which was not the case prior to 1950. In the 3–6 year band, central streamflow is essentially depicted by the NAO since 1970 and by the PNA before 1970. In general, the Canadian streamflow activity in the 3–6 year band is depicted by the NAO, the ENSO3, and the PNA. The correlation analysis results confirm that NAM and NAO can have significantly different impacts in a given region, indicating that the two climatic patterns are not identical. The wavelet analysis results also indicate that streamflow regionalization can be refined based on their wavelet spectra. Further analysis should include monthly streamflows and climatic patterns to assess high-frequency (infra-annual/seasonal) structures.

Table 2. Correlation Analysis Results for the 2–3 Year Band

Climate Indices	≤1950	≥1950	≤1970	≥1970	1911–1999[a]
		West			
ENSO3	−0.19	0.46	0.45	0.35	0.52
NAO	0.09	−0.38	0.24	−0.24	−0.14
NAM	0.36	−0.29	0.34	−0.33	−0.08
PNA	–	−0.16	−0.08	−0.47	−0.15
		Central			
ENSO3	0.28	−0.50	−0.15	0.07	0.05
NAO	0.18	0.03	0.21	0.01	0.16
NAM	0.01	−0.31	−0.20	0.39	0.15
PNA	–	−0.24	−0.55	−0.01	−0.24
		East			
ENSO3	−0.14	−0.04	−0.06	−0.48	0.24
NAO	0.11	−0.64	0.15	−0.40	−0.17
NAM	0.53	−0.18	0.38	0.18	0.12
PNA	–	0.66	−0.37	0.57	0.66
		All			
ENSO3	−0.07	−0.27	−0.17	−0.16	−0.08
NAO	0.31	0.26	0.20	−0.55	0.01
NAM	0.62	−0.27	0.40	−0.06	0.29
PNA	–	0.47	−0.40	0.53	0.48

[a]Except for the PNA index, where time series are available for 1950–1999.

Table 3. Correlation Analysis Results for the 3–6 Year Band

Climate Indices	≤1950	≥1950	≤1970	≥1970	1911–1999[a]
		West			
ENSO3	0.15	−0.48	−0.08	−0.63	0.04
NAO	0.48	−0.69	−0.38	−0.67	−0.12
NAM	−0.01	−0.20	−0.04	−0.56	−0.14
PNA	–	−0.59	−0.62	−0.64	−0.56
		Central			
ENSO3	−0.22	0.03	−0.08	−0.18	0.14
NAO	−0.11	−0.05	−0.20	−0.46	−0.18
NAM	−0.38	−0.34	−0.28	−0.20	−0.26
PNA	–	0.01	0.75	−0.35	0.01
		East			
ENSO3	0.04	−0.66	−0.08	−0.70	−0.17
NAO	0.36	−0.73	0.20	−0.79	0.14
NAM	−0.18	−0.26	−0.21	−0.19	−0.20
PNA	–	−0.47	−0.84	−0.32	−0.45
		All			
ENSO3	−0.65	−0.70	−0.61	−0.62	−0.58
NAO	−0.64	−0.52	−0.62	−0.58	−0.61
NAM	−0.45	−0.09	−0.37	−0.38	−0.34
PNA	–	−0.53	0.40	−0.40	−0.53

[a]Except for the PNA index, where time series are available for 1950–1999.

[35] **Acknowledgments.** This work was made possible through grants from the Natural Sciences and Engineering Research Council of Canada to each author. The authors gratefully acknowledge the student contribution of Vanessa Arnold. Main wavelet analysis routines were provided by C. Torrence and G. P. Compo, and are available at http://paos.colorado.edu/research/wavelets/. The NAO, PNA, and ENSO3 indices are available through NOAA's Climate Prediction Center at http://www.cpc.ncep.noaa.gov/. The NAM (or AO) index values are available through D. W. J. Thompson's Annular Modes Web site at URL: http://www.atmos.colostate.edu/ao/.

References

Adamowski, K., and C. Bocci (2001), Geostatistical regional trend detection in river flow data, *Hydrol. Processes*, *15*, 3331–3341.

Ambaum, M. H. P., B. J. Hoskins, and D. B. Stephenson (2001), Arctic Oscillation or North Atlantic Oscillation?, *J. Clim.*, *14*, 3495–3507.

Barnston, A. G., and R. E. Livezey (1987), Classification, seasonality and persistence of low-frequency atmospheric circulation patterns, *Mon. Weather Rev.*, *115*, 1083–1126.

Brown, R. D. (1995), Spatial and temporal variability of North American snow cover, 1971–1992, paper presented at the 52nd Eastern Snow Conference, Toronto, Ont., Canada.

Brown, R. D., and B. E. Goodison (1996), Interannual variability in reconstructed Canadian snow cover, 1915–1992, *J. Clim.*, *9*, 1299–1318.

Cayan, D. R. (1992), Latent and sensible heat flux anomalies over the northern oceans: The connection to monthly atmospheric circulation, *J. Clim.*, *5*, 354–369.

Chen, H. L., and A. R. Rao (2002), Testing hydrologic time series for stationarity, *J. Hydrol. Eng.*, *7*, 129–136.

Cook, E. R., R. D. D'Arrigo, and K. F. Briffa (1998), A reconstruction of the North Atlantic Oscillation using tree-ring chronologies from North America and Europe, *Holocene*, *8*, 1–9.

Coulibaly, P., F. Anctil, P. Rasmussen, and B. Bobée (2000), A recurrent neural networks approach using indices of low-frequency climatic variability to forecast regional annual runoff, *Hydrol. Processes*, *14*, 2755–2777.

Daubechies, I. (1990), The wavelet transform time-frequency localization and signal analysis, *IEEE Trans. Inf. Theory*, *36*, 961–1004.

Diaz, H. F., M. P. Hoerling, and J. K. Eischeid (2001), ENSO variability, teleconnections and climate change, *Int. J. Climatol.*, *21*, 1845–1862.

Dracup, J. A., and E. Kahya (1994), The relationships between U.S. streamflow and La Niña events, *Water Resour. Res.*, *30*, 2133–2141.

Eltahir, E. A. B. (1996), El Niño and the natural variability in the flow of the Nile River, *Water Resour. Res.*, *32*, 131–137.

Gutiérrez, F., and J. A. Dracup (2001), An analysis of the feasibility of long-range streamflow forecasting for Columbia using El Niño-Southern Oscillation indicators, *J. Hydrol.*, *246*, 181–196.

Harvey, K. D., P. J. Pilon, and T. R. Yuzyk (1999), Canada's Reference Hydrometric Basin Network (RHBN), in *Proceedings of the CWRA 51st Annual Conference*, Can. Water Resour. Assoc., Cambridge, Ont., Canada.

Higuchi, K., J. Huang, and A. Shabbar (1999), A wavelet characterization of the North Atlantic Oscillation variation and its relationship to the North Atlantic sea surface temperature, *Int. J. Climatol.*, *19*, 1119–1129.

Hu, Q., C. M. Woodruff, and S. E. Mudrick (1998), Interdecadal variations of annual precipitation in the central United States, *Bull. Am. Meteorol. Soc.*, *79*, 221–229.

Huang, J., K. Higushi, and A. Shabbar (1998), The relationship between the North Atlantic Oscillation and the El Niño-Southern Oscillation, *Geophys. Res. Lett.*, *25*, 2707–2710.

Hurrell, J. W. (1995), Decadal trends in the North Atlantic Oscillation: Regional temperature and precipitation, *Science*, *269*, 676–679.

Hurrell, J. W., Y. Kushnir, G. Ottersen, M. Visbeck (Eds.) (2003), *The North Atlantic Oscillation: Climatic Significance and Environmental Impact, Geophys. Monogr. Ser.*, vol. 134, 279 pp., AGU, Washington, D. C.

Kahya, E., and J. A. Dracup (1993), U.S. streamflow patterns in relation to the El Niño-Southern Oscillation, *Water Resour. Res.*, *29*, 2491–2503.

Kaiser, G. (1994), *A Friendly Guide to Wavelets*, 300 pp., Birkhäuser Boston, Cambridge, Mass.

Kiem, A. S., and S. W. Franks (2001), On the identification of ENSO-induced rainfall and runoff variability: A comparison of methods and indices, *Hydrol. Sci. J.*, *46*, 715–727.

Kumar, P. (1996), Role of coherent structure in the stochastic dynamic variability of precipitation, *J. Geophys. Res.*, *101*, 393–404.

Kumar, P., and E. Foufoula-Georgiou (1993), A multicomponent decomposition of spatial rainfall fields: Segregation of large- and small-scale features using wavelet transforms, *Water Resour. Res.*, *29*, 2515–2532.

Labat, D., R. Ababou, and A. Mangin (2000), Rainfall-runoff relations for karstic springs: Part II. Continuous wavelet and discrete orthogonal multiresolution analyses, *J. Hydrol.*, *238*, 149–178.

Lamb, P. J., and R. A. Peppler (1987), North Atlantic Oscillation: Concept and application, *Bull. Am. Meteorol. Soc.*, *68*, 1218–1225.

Lucero, O. A., and N. C. Rodriguez (1999), Relationship between interdecadal fluctuations in annual rainfall amount and annual rainfall trend in a southern mid-latitudes region of Argentina, *Atmos. Res.*, *52*, 177–193.

McKerchar, A. I., C. P. Pearson, and M. E. Moss (1996), Prediction of summer inflows to lakes in the Southern Alps, New Zealand, using the spring Southern Oscillation Index, *J. Hydrol.*, *184*, 175–187.

Moss, M. E., C. P. Pearson, and A. I. McKerchar (1994), The Southern Oscillation Index as a predictor of the probability of low streamflows in New Zealand, *Water Resour. Res.*, *30*, 2713–2717.

National Research Council (1998), *Decade-to-Century-Scale Climate Variability and Change: A Science Strategy*, 142 pp., Natl. Acad. Press, Washington, D. C.

Perreault, L., J. Bernier, B. Bobée, and E. Parent (2000), Bayesian change-point analysis in hydrometeorological time series: Part 1. The normal model revised, *J. Hydrol.*, *235*, 221–241.

Piechota, T. C., and J. A. Dracup (1999), Long-range streamflow forecasting using El Niño-Southern Oscillation indicators, *J. Hydrol. Eng.*, *4*, 144–151.

Piechota, T. C., J. A. Dracup, and R. G. Fowell (1997), Western U.S. streamflow and atmospheric circulation patterns during El Niño-Southern Oscillation (ENSO), *J. Hydrol.*, *201*, 249–271.

Piechota, T. C., F. H. S. Chiew, and J. A. Dracup (1998), Seasonal streamflow forecasting in eastern Australia and the El Niño-Southern Oscillation, *Water Resour. Res.*, *34*, 3035–3044.

Rajagopalan, B., and U. Lall (1998), Interannual variability in western U.S. precipitation, *J. Hydrol.*, *210*, 51–67.

Rasmusson, E. M., and T. H. Carpenter (1982), Variations in tropical sea surface temperature and surface wind fields associated with the Southern Oscillation/El Niño, *Mon. Weather Rev.*, *110*, 354–384.

Redmond, K. T., and R. W. Koch (1991), Surface climate and streamflow variability in the western United States and their relationships to large-scale circulation indices, *Water Resour. Res.*, *27*, 2381–2399.

Saco, P., and P. Kumar (2000), Coherent modes in multiscale variability of streamflow over the United States, *Water Resour. Res.*, *36*, 1049–1067.

Serreze, M. C., J. E. Walsh, F. S. Chapin III, T. Osterkamp, M. Dyurgerov, V. Romanovsky, W. C. Oechel, J. Morison, T. Zhang, and R. G. Barry (2000), Observational evidence of recent change in the northern high-latitude environment, *Clim. Change*, *46*, 159–207.

Shabbar, A., B. Bonsal, and M. Khandekar (1997a), Canadian precipitation patterns associated with the Southern Oscillation, *J. Clim.*, *10*, 3016–3027.

Shabbar, A., K. Higuchi, W. Skinner, and J. L. Knox (1997b), The association between the BWA index and winter surface temperature variability over eastern Canada and west Greenland, *Int. J. Climatol.*, *17*, 1195–1210.

Smith, J. A. (1992), Representation of basin scale in flood peak distribution, *Water Resour. Res.*, *28*, 2993–2999.

Smith, L. C., D. Turcotte, and B. L. Isacks (1998), Stream flow characterization and feature detection using a discrete wavelet transform, *Hydrol. Processes*, *12*, 233–249.

Szilagyi, J., M. B. Parlange, G. G. Katul, and J. D. Albertson (1999), An objective method for determining principal time scales of coherent eddy structures using orthogonal wavelets, *Adv. Water Resour.*, *22*(6), 561–566.

Takeuchi, N., K. Narita, and Y. Goto (1994), Wavelet analysis of meteorological variables under thunderclouds over the Japan sea, *J. Geophys. Res.*, *99*, 10,751–10,757.

Thompson, D. W. J., and J. M. Wallace (1998), The Arctic Oscillation signature in the wintertime geopotential height and temperature fields, *Geophys. Res. Lett.*, *25*, 1297–1300.

Thompson, D. W. J., and J. M. Wallace (2000), Annular modes in the extratropical circulation: Part I. Month-to-month variability, *J. Clim.*, *15*, 1000–1016.

Thompson, D. W. J., and J. M. Wallace (2001), Regional climate impacts of the Northern Hemisphere annular mode and associated climate trends, *Science*, *293*, 85–89.

Torrence, C., and G. P. Compo (1998), A practical guide to wavelet analysis, *Bull. Am. Meteorol. Soc.*, *79*, 61–78.

Torrence, C., and P. J. Webster (1999), Interdecadal changes in the ENSO-monsoon system, *J. Clim.*, *12*, 2679–2690.

Wallace, J. M. (2000), North Atlantic Oscillation/annular mode: Two paradigms, one phenomenon, *Q. J. R. Meteorol. Soc.*, *126*, 791–805.

Wallace, J. M., and D. S. Gutzler (1981), Teleconnections in the geopotential height field during the Northern Hemisphere winter, *Mon. Weather Rev.*, *109*, 784–812.

Yarnal, B., and H. F. Diaz (1986), Relationships between the extremes of the Southern Oscillations and the winter climate of the Anglo-American Pacific coast, *Int. J. Climatol.*, *6*, 197–219.

D. H. Burn, Department of Civil Engineering, University of Waterloo, Waterloo, Ont., Canada N2L 3G1. (dhburn@uwaterloo.ca)

P. Coulibaly, Department of Civil Engineering, McMaster University, Hamilton, Ont., Canada L8S 4L7. (couliba@mcmaster.ca)